Aalborg Universitet

The Feasibility of Communication Among Pumps in a District Heating System

Meybodi, Soroush Afkhami; Dohler, Mischa; Askarpour, Amir Nader; Bendtsen, Jan Dimon; Nielsen, Jens Frederik Dalsgaard

Feasibility of Communication among Pumps in a District Heating System

Soroush Afkhami Meybodi [1], Mischa Dohler [2], Jan Bendtsen [3], Jens Dalsgaard Nielsen [4],

[1,3,4]*Department of Electronic Systems, Aalborg University*
Fredrik Bajers Vej 7C, Aalborg, Denmark – Phone: +45 99408702, Fax: +45 98151739

[2]*Centre Tecnolgic de Telecomunicacions de Catalunya*
Av. Carl Friedrich Gauss 7, Castelldefels, Spain – Phone: +34 679094007, Fax: +34 936452901

{[1]sam, [3]dimon, [4]jdn}@es.aau.dk

[2]mischa.dohler@cttc.es

Abstract—The tackled problem is: selecting a viable method for communication among pumps in a district heating system, viewed as a metropolitan wireless sensor network whose nodes are confined underground and physically connected by pipes. In a further horizon, providing sophisticated control systems for similar urban utilities motivates this research problem. Here, we have reported the results of investigating several potential methods for realizing the idea of "The Talking Pumps" in a district heating system. This includes a diverse list of key references, simulations for some methods, and experimental results for some others, followed by selection the most appropriate option. The considered methods are using 1) Acoustic waves through water and pipelines, 2) Power line communications, 3) Electrical conductivity of pipes, 4) Cell phone infrastructure, 5) Free and guided Radio Frequency (RF) Electromagnetic (EM) waves, and 5) free and guided Very Low Frequency (VLF) electric and magnetic fields, also known as Magnetic Induction. The viability of the latter is verified by simulations and primitive experimental results.

Keywords: *Electromagnetic propagation in absorbing media, Propagation losses, Electromagnetic induction, Near-field radiation pattern, Coil antenna design*

I. INTRODUCTION

Advances in the fields of Wireless Sensor Networks (WSN) and Networked Control Systems (NCS) have created many new opportunities for joint designs where a control system routes its required signals via wireless communication links. Specific applications are emerging among urban utilities and infrastructure e.g. water distribution systems [1-3] and district heating systems (DHS) [4]. Unlike electricity distribution, another urban utility, that needs a sophisticated dispatching control with access to real time network-wide data to prevent instabilities, the above mentioned utilities may work well by making use of local simple controllers, in expense of fairly low energy efficiency [5]. However, ever-increasing energy prices and environmental concerns have leveraged the technological advances toward more energy saving solutions. Our focus in this paper is on the feasibility of a communication framework that is going to host the control system for a district heating plant.

District heating is a method for providing heat demands to closely located buildings by delivering hot water to them and cycling the return cooled water into heating plants via dedicated pair-wise pipelines. They create a closed pressurized hydronic system in which water flows by centrifugal pumps. Pipes are buried underground and pumps are usually placed in the basement of buildings along the pipes. They are wired to local pressure sensors to provide local control of the hydronic dynamics. In the traditional design (Fig. 1), there are a few pumps for many end users.
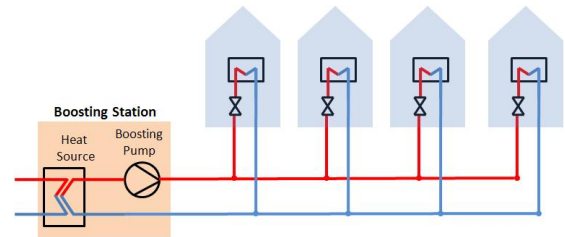

Fig. 1.   District heating piping layout: The traditional design

Assuming a minimum pressure across all end users is required, each pump should be operated based on the differential pressure across the farthest end user [6]. Measured pressure of the farthest end user is currently transmitted over internet at prescribed time intervals. A human operator uses this data besides weather conditions and weather forecast, to roughly change the pump operating settings. A drawback of such a control method is the considerable loss of pumping energy due to presence of pressure reducing valves across end users which are located close to the pump. Furthermore, the diameters of pipes are optimized and chosen large enough to prevent pressure loss in far loads. This increases heat loss due to large pipe diameters and deteriorates overall energy efficiency.

In a newly proposed piping layout [5] which is designed to improve energy efficiency, the number of pumps are increased and cooperation among them is mandatory to maintain stability of the hydronic network (Fig. 2).

The goal is to divide the burden of the big old pump among smaller new pumps in an optimal manner. The new pumps are to be placed at each end user and in boosting stations. This layout results in saving pumping energy and facilitates the use of pipes with smaller diameters in future installations, hence contributes to heat loss alleviation. On the other hand, this structure requires data communication among pumps, e.g. data
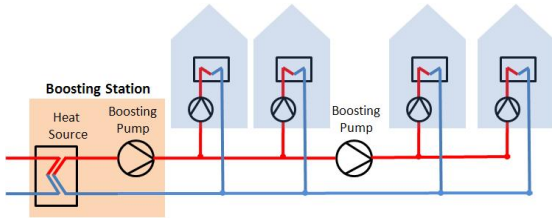
Fig. 2.   District heating piping layout: New design

from end user pumps must be sent to their upstream boosting pump [7].

Signaling among the pumps is not trivial. They are located in buildings' basements, which are typically air-filled underground chambers with concrete walls. Pipes are already laid and there is no chance to add wires along them to connect them together.

In a previous paper [8], we investigated the required coverage range of a host wireless network by extracting the empirical cumulative distribution function (CDF) of pumps' inter-distances. We found that a range of 40 m provides at least one in-range neighbor for each pump, while 60% of the pumps have 5 accessible neighbors. Although it does not guarantee full connectivity for the network graph from mathematical point of view, it gives acceptable results in commonplace piping layouts. Therefore, our goal in this paper is to choose and verify a communication method for a typical 40 m through-soil range of an underground network.

Several methods have been tried in the literature to solve similar problems, but there is still no outstanding solution. Section II introduces these methods. Cited references are in some cases backed by simulations, experiments, and feasibility assessment which contribute to prove inadequacy of the inspected methods.

The main focus of the paper is on *Magnetic Induction (MI)* which is introduced in Section III. MI has already found several applications. It is used in very low power wireless microphones and headsets that are used by security forces [9-11] in frequency ranges 11-15 MHz and distances up to 3 m providing a high level of security by involving quasi-static fields - to be described later. Lower frequencies of 300 Hz to 4 KHz are employed for distances up to a few kilometers in soil or water medium. They have been used in underground and underwater voice and data communications for mining and military purposes, underwater navigation, remote triggering of underground and underwater mines and ammunition, seismic fence, and submarine communication systems [12-15]. We will see later in this paper, that in such cases the communication media are hardly penetrable by higher frequencies.

Section IV contains a simulation study on optimal design of MI transceiver antennas. It is followed by experimental results in Section V which confirm viability of MI for making underground communication links of the required range. Section VI concludes the paper.

II. Various Communication Technologies for District Heating

A. Radio frequency electromagnetic waves

This method makes use of Industrial, Scientific, and Medical (ISM) unlicensed radio bands and employs them for underground communications. In contrast to above-ground systems, the main challenge in *Physical* layer is coverage rather than interference mainly because of the high propagation losses of EM waves through the soil [16].

1) through-the-soil communications: The maximum transmission range of RF systems depends on transmission power, antenna gains, propagation losses and receiver sensitivity. Propagation losses in a homogenous environment consist merely of pathloss which depends on dielectric properties of the medium and the distance between transmitter and receiver. Dielectric properties of soil depend highly on the soil composition and water content [17, 18] that varies quite a lot for different locations and from time to time. This results in a large uncertainty in pathloss behavior besides its typical large value.

Reference [19] gives insight to the maximum achievable transmission range with different frequencies, transmission powers and volumetric water contents of soil. It is shown that the range can be extended only up to 4 m with 10^{-3} BER for nodes buried in a depth more than 2 m, assuming operating frequency of 400MHz, 30 dBm power transmission, volumetric water content of 5%, and PSK modulation which are all quite good conditions. More water content and higher frequencies exacerbate the result. However, this range is certainly inadequate for our problem.

2) Combined underground above-ground: The nodes in our network are not buried, but merely placed in basements. This provides a chance for creating multiple paths for a signal, through walls from basement to surface, transmission above the surface, and through walls from surface to basement again at the destination. In an unrealistic ideal condition depicted in Fig. 3, i.e. with the existence of ideal reflecting surfaces above ground, EM waves should penetrate at least through four thick walls.

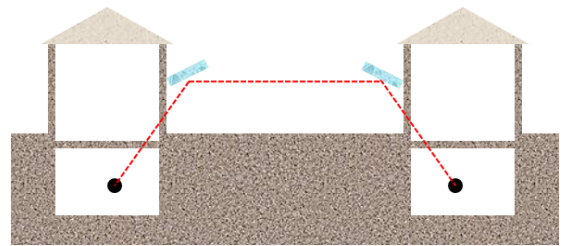Fig. 3.   A typical underground above-ground combined scenario

Based on the empirically derived pathloss models in [20] which are valid for the operating frequencies of 2-6 GHz, we have estimated pathloss as a function of horizontal distance between the transmitter and the receiver for a set of frequencies. The arrangement in Fig. 3 is similar to the indoor room-to-room scenario in [20] with four thick walls.

For this scenario, pathloss (PL) can be estimated as follows:

$$PL[dB] = \quad 20\log_{10}(d[m]) + 46.4$$
$$+20\log_{10}\left(\frac{f[GHz]}{5.0}\right) + 12n_w \quad (1)$$

where d is the distance between transceivers, f is the operating frequency, and n_w is the number of thick walls [20]. The results are shown in Fig. 4.
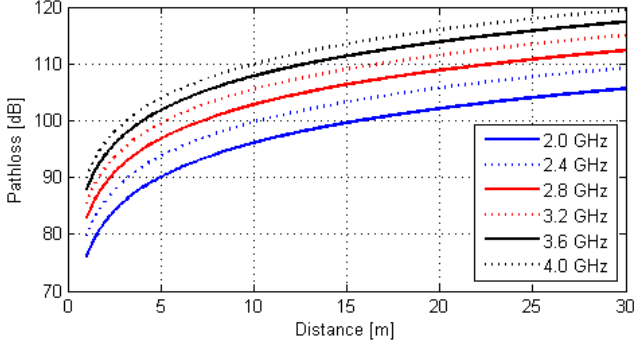

Fig. 4.   Pathloss vs. horizontal distance for several frequencies

Fig. 4 suggests a maximum transmission range of 15 m in ideal conditions, assuming a maximum tolerable signal loss of 100 dB, which is the dynamic range of current embedded radios. It is still less than the required range of 40 m, but it also shows that there could be a chance if lower frequencies are employed. However, (1) is not valid for $f <$2.0 GHz.

To see if lower frequencies can be useful, we ran a test with APC220 radio modules tuned at 434MHz. The selected frequency is the lowest unlicensed frequency that could be supported by APC220 radio. The sensitivity of this radio is -112dB at 9600 bps, and it uses GFSK modulation.

The experiment was a simple broadcast test. The transmitter was fixed in a basement, broadcasting a life signal once every second. The receiver, which was a mobile node, was listening to the life signals. We started with both nodes placed close to each other, then got out of the basement with the receiver node and moved towards the neighboring basement located in 10 m distance. It turned out that as soon as we were to go down in the second basement, the life signal was completely lost. This result is due to the lack of the required reflecting surfaces in real scenarios. We did not pursue this approach any further.

3) Pipelines as waveguides: Another idea is to combine the ubiquitous embedded radios with the potential waveguide properties of the pipes. The question is whether a water filled pipe can act as an efficient waveguide. Although it has already been investigated with air filled metallic ducts with some degrees of success [21], there is a skepticism regarding water as the inner material. An EM waveguide principally consists of either two dielectric materials, i.e. a *dielectric waveguide* or a metal and an insulator, i.e. a *matallic waveguide*, but if none of the materials is an insulator, the wave cannot be propagated through the tube.

Water, as is used in district heating, is neither a good conductor, nor a good insulator. Its conductivity is less than 10^{-3} S/m [6] compared to 2.0×10^6 S/m for steel [22] and 0.3×10^{-14} to 0.8×10^{-14} S/m [23] for air. These numbers motivated us to do a simple experiment to measure attenuation in a water filled pipe presumed as a waveguide.

The experiment setup is shown in Fig. 5. We used a 2.5" iron pipe conforming to DIN2440 standard. It was integrated into the potable water distribution pipelines. As the transmitter and the receiver, we used coil antennas each made of 83 turns of single layered insulated copper wire conforming to AWG 30 standard. Lengths of the coils turned out to be 40 mm. Both antennas were shielded in cardboard boxes which were totally covered by a thick aluminum foil. Therefore, the signal could only transmit through the pipe.
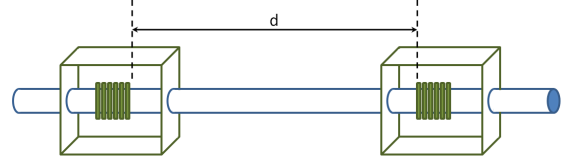

Fig. 5.   Metallic waveguide experiment setup

The coils were connected to a *Signal Generator* and a *Spectrum Analyzer* without impedance matching circuits. Fig. 6 shows signal loss as a function of distance (d) between the coils for operating frequency 400 MHz. Impedance mismatch of the two circuits imposes a large constant signal loss, but we are generally interested in the variations of signal loss versus d. Therefore, it is possible to ignore the matching problem assuming that the matching parameters are not affected considerably while d varies.
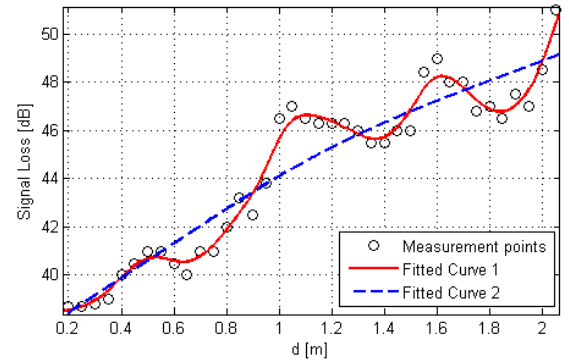
Fig. 6.   Waveguide effect on signal loss at 400 MHz

The oscillatory behavior of signal loss admits existence of the waveguide effect. The observed wavelength is approximately 0.5-0.6 m which is in accordance with the calculated wavelength for 400 MHz in water medium, i.e. 0.56 m, provided that:

$$v = \frac{c}{n} \quad (2)$$
$$\lambda = \frac{v}{f}$$

where c (2.9979×10^8 m/s) is the speed of light in vacuum, n (1.333) is the *index of refraction* of water, v is the speed of light in water, λ is the wavelength, and f is the operating frequency [22].

Measured data are smoothed and plotted in Fig. 6 in two steps. The first fit explicitly shows the oscillatory behavior,

while the second fit shows the general trend and anticipates, via extrapolation, 100 dB of signal loss at approximately 20 m after impedance matching. Unfortunately, we did not have access to longer straight water filled pipes to verify this result, but it is not satisfying for our DHS problem yet, considering the required range of 40 m and the presence of bends and branches in pipes, in practice, which severely affect the waveguide properties.

B. Acoustic waves

Another intuitive option is to exploit the infrastructure itself as the communication medium. One way is to employ mechanical vibrations in form of sonic/ultrasonic waves as the carrier of data. Either pipes or water could be used as the main medium. There is an intrinsic advantage in using water because there could be variations in the material of the pipes in some cases in practice. However, we have considered both cases.

1) Acoustics through the water: Using water as the main communication medium has received less attention compared to in-pipe propagation. Sound speed in water is about 27% of in iron, i.e. 1500 m/s versus 5500 m/s [24]. Therefore, the wavelength at the same frequency is shorter with the same proportion, making the wave more prone to destructive multipath effect. *Doppler Effect* is also another issue since the speed of water is comparable with the speed of sound [25].

The most successful application in this area is underwater open-sea communication where the multipath effect is minimized. Usages are including oceanography, environmental monitoring, *tsunami* warning, etc. [26] with commercial products.

2) Acoustics through the pipes: Besides pipe's material and geometry, propagation of sound waves in a pipe depends on the materials inside and outside of it. The simplest results are achieved if there is vacuum inside and out. Simulation and experimental results are reported for gas filled pipes in [27]. The application is remote reading of meters for natural gas distribution companies [28]. A two-way data transmission rate of 2560 bps is reported with 1×10^{-2} bit error rate (BER) for transmission via a typical six floor building with branches and bends in pipes, assuming in-line speakers and microphones. However, no commercial products were traced at the time of writing this article.

Wave propagation in water filled pipes is investigated in [24, 29, 30]. The second chapter of [29] offers a clear and compact literature review on the subject, while [24] gives a detailed analysis of the dispersion of different acoustic modes in a water filled pipe. Open-sea and in-pipe cases are compared in [30]. All of these references state that the main source of signal attenuation in pipes is reverberation which depends heavily on the geometry, fittings, bends and branches of the pipes, hence are totally different from one case to another.

The most successful relevant application is pipe leak detector [30] which is not a two way communication system and requires a low data rate. In such commercialized systems, microphones are installed on pipes with prescribed distances. They listen for a continuous noise which will be interpreted as the aftermath of water leakage from a pipe breakage. Provided that there is a synchronizing facility among microphones, which needs another means of communication among them, location of the breakage can be calculated by measuring the differences of time-of-arrivals of signals.

Experimental results [30] for steel pipes with the diameter of 10 cm, predict the un-coded BER 32% for data sent at the rate of 7 kbps at 21 kHz with FSK modulation in a straight buried pipe. The transmitter and receiver are located approximately 9 m away from each other. Although BER could be remedied by signal processing techniques, the transmission range is obviously insufficient. Furthermore, the microphone and speaker which were used in this experimental study were installed inside the pipe and precisely centered at the pipe axis. However, in practice, clamped equipments are preferred than flanged or threaded ones due to feasibility and maintenance considerations.

Last but not least, the communication framework that we are interested to build is going to host a control system for regulating pressure and compensating pressure disturbances in a DHS. This means that the transmitted data have the highest importance when pressure irregularities happen, but these irregularities also induce vibrational noise which degrades reliability of the communication link. Therefore, the channel is least usable when it is most needed.

Marginal reported experimental results for short pipes, the high price of the required hardware, i.e. comparable to the price of the pump itself, and the effect of the process disturbance on the communication channel makes the current acoustic technologies unreliable for in-pipe communications.

C. Electrical conductivity

1) Power line communications: Power Line Communications (PLC) makes use of the power grid as a wireline network for data transfer. The idea has been around since 1920's for voice communication, telemetry, and supervisory control [31]. The technology was revisited two times: 1)in late 1970's, motivated by the advent of digital signal processing, in order to be used as a means of load management and remote meter reading in electrical networks [32]; and 2)in late 1990's to host broadband services like internet over power lines [33].

The main drawback of using PLC is the variety of applications and non-interoperable standards which are thriving and competing to gain access to the readily available power grid infrastructure. Such a competition has become harsher than ever by the advent of Smart Grid. A comprehensive and recent study on applications and standards can be found in [34]. Urban utilities, including electrical power distribution, water distribution, gas distribution, and district heating are not considered so far to use PLC in any application other than automatic metering. Therefore, finding space for bandwidth demanding applications like real time control of such plants involves lots of lobbying and non-technical settlements.

There are some technical difficulties in relying on PLC too. Frequency ranges in PLC start from a few hundred hertz for long distance narrow-band applications up to 200 MHz for home applications with a very short range and high bandwidth.

The power grid is designed for 50-60 Hz which raises EMC considerations and mutual interference for employment of higher frequencies, especially for those more than 80 MHz due to the presence of ubiquitous TV broadcast channels. This fact has limited the permissible transmission power and has put off the standardization processes.

Another problem is the existence of transformers in power networks which filter out high frequencies. Therefore, bypass devices are needed to be installed in parallel with transformers [35]. It explains why PLC has been mostly successful in home automation and intra-building control systems where there is no electrical isolation; and low transmission powers can still cover the required range.

In a DHS, nodes are geographically dispersed and could be located in areas supplied by different transformers. Without the use of bypass devices, a partitioning is imposed on the network which is probably not in agreement with the control system structure. If we accept this major limitation, PLC is a feasible low bandwidth solution, at least from the technical point of view, but maybe not a timely solution due to the lack standards for our specific application and interference with other existing systems.

2) Pipes as wires: This is another intuitive and cheap solution, provided that the pipes are all metallic and electrical conductivity is preserved across the fittings. The idea is to use the conductive pipes as electrical wires. There is only one major problem, i.e. Grounding.

In water distribution systems, pipes are in contact with the soil either directly or through their thin layered coating. This forms a frequency dependent electrical resistance (R_{leak}) between the pipe and earth, as the electrical ground. Large R_{leak} is desired at the operating frequency. There is also another frequency dependent electrical resistance (R_{pipe}) between two neighboring nodes on the pipes. It is shown that with an appropriate use of the skin effect, by choosing the right operating frequency such that R_{leak}/R_{pipe} is maximized, it is possible to make use of this leaky multi-ground system to send and receive signals [36].

However, in a DHS, pipes are heavily insulated with foam-filled PVC jackets in order to prevent heat loss. Therefore, they are required to be grounded with copper wires as they enter each basement to hamper electrostatic shock hazards. Moreover, a simple calculation of skin depth shows that the skin depth of steel (pipes' material) is significantly less than copper (earth wire) [22]. Therefore, increasing the frequency will even aggravate the attenuation by increasing R_{pipe}/R_{leak}.

In summary, dependency on pipes' material, direct grounding of pipes, and the stronger skin effect for pipes compared to earth wires, diminish any chance to transfer signals through the pipe by this method.

D. Cell phone infrastructure

There are lots of commercial products and some publications which claim to offer remote monitoring and control of home appliances by mobile phones. The idea is to use two SIM cards and transfer data by Short Message Service (SMS). It works well, when a single measurement or command needs to be sent. Switching home appliances ON and OFF, sending an alarm signal from the field to a remote operator, or automatic reading of electricity/water/heating meters once a month/year are among success stories, but it cannot be applied to our closed loop control problem due to the following concerns.

First of all, the system will be dependent on a third party infrastructure which is not desirable. Second, in every closed control loop, signaling should be fast enough compared to the dynamics of the measured variable, i.e. water pressure in our case. In hydronic systems, changes in water pressure propagate with the speed of sound in pipes, which is 1500 m/s. Comparing this speed with typical distances in an urban area suggests a sampling rate in order of 1 Hz. Sending a SMS at every second is quite expensive, if possible. Third, from technical point of view, SMS is sent via signaling paths which are originally provided to control the telephony traffic. They are separate from main voice path and have a maximum payload capacity of 1120 bits. The signaling paths let SMS go through whenever no higher priority traffic control signal exists. Therefore, congestion can happen resulting in a varying delay of several seconds. SMS centers store and retry to forward old messages by default. This function exacerbates the situation by making a long queue at the SMS center.

Furthermore, our application requires the nodes to be placed in the basement of buildings where signal strength is greatly attenuated even for well covered cellular networks. Based on authors' observations, even in automatic reading of meters which is a quite successful application for cellular monitoring, regular human operator check is required when the apparatus is located in the basement.

III. MAGNETIC INDUCTION

MI has been around since 1920's being used as a means of communication between submarines [14]. There is no fundamental difference between MI and RF EM waves. However, because of different technical specification, most importantly antenna size, available bandwidth and transmission power, various names have popped up to describe it including *Very Low Frequency (VLF)*, *Ultra Low Frequency (ULF)*, and *Extremely Low Frequency (ELF)*. Each of these names addresses a certain range of frequencies which are not even understood in the same way, in different communities. For example, *National Aeronautics and Space Administration (NASA)*, *World Health Organization (WHO)*, and *International Telecommunication Union (ITU)* have all assigned different frequency ranges to define the above terms. In this article, we use MI as the only alternative term and explain why it is worth being distinguished from usual radio spectrum.

MI also employs alternating Electric (**E**) and Magnetic (**B**) fields as data carrier, but it uses low frequencies and low power such that the communication range falls off within the distance predominated by the *static* or *quasi-static* fields, as described in the following.

E and **B** fields which are created by an alternating electrical current in an antenna can be estimated by the summation of several terms that have different dependencies to distance r from the antenna, e.g. $|\mathbf{B}| \approx \alpha.1/r^3 + \beta.1/r^2 + \gamma.1/r$ in

which α, β, and γ depend on the antenna pattern and its driving current. In the vicinity of the antenna, fields are very complex (to be shown later in Section IV). Gradually, they are predominated by $1/r^3$ term. Up to this zone, is called the *static field* domain. Other terms predominate at farther distances and are called *inductance field (quasi-static field)* and *radiation field*, respectively [22]. The latter accounts for EM radiation in which $|\mathbf{B}| \propto 1/r$ and $|\mathbf{E}| \propto 1/r$. To define which field component is predominant, r should be compared with *wave number, k*:

$$k = \omega/v \tag{3}$$

where ω is the angular frequency of the $\mathbf{E}$ and $\mathbf{B}$ fields and v is speed of EM waves in the medium. $k.r \gg 1$ and $k.r \ll 1$ imply that either the radiation or the static field is dominant, respectively. Otherwise, the field is quasi-static.

Static and quasi-static fields decay much faster than the radiation field while getting away from the current source. More concretely, their energy flux *Poynting Vector* decays faster than $1/r^2$ and the emitted power per area tends to zero as distance from the source goes to ∞. Therefore, they are non-radiating fields and have no value in long range communications. However, if the frequency is low enough, the distances of interest can still be perceived as short distances. Hence, even non-radiating fields can be exploited to transfer energy between transceivers. In our underground communication problem, the choice of the operating frequency leaves us in non-radiating field domain.

Why should we choose such low operating frequencies? The answer lies in the dielectric properties of lossy materials like wet soil. When materials are influenced by alternating $\mathbf{E}$ and $\mathbf{B}$ fields, their electric susceptibility (χ_e) can be stated as a complex function of frequency:

$$\chi_e(\omega) = \chi_e'(\omega) - j\chi_e''(\omega) \tag{4}$$

The general behavior of real part $\chi_e'(\omega)$ and imaginary part $\chi_e''(\omega)$ for most of the materials is sketched in Fig. 7 [37]. $\chi_e'(\omega)$ increases most of the times with respect to ω, except for short intervals where it drastically decreases. These intervals coincide with local maxima in $\chi_e''(\omega)$. $\chi_e'(\omega)$ defines velocity of $\mathbf{E}$ and $\mathbf{B}$ fields in a matter, while $\chi_e''(\omega)$ accounts for attenuation due to molecular resonance phenomena. It
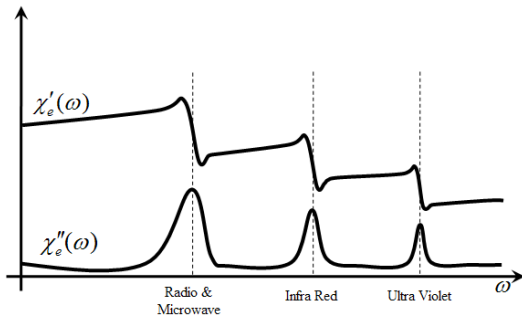

Fig. 7.   Electrical susceptibility of matters versus frequency

provides an extra *alternating field conductivity* (σ_a) besides the common *static field conductivity* (σ_s) at resonance frequencies. The overall conductivity (σ_e) can be stated as [37]:

$$\sigma_e = \sigma_s + \sigma_a = \sigma_s + \omega(\epsilon_0 \chi_e''(\omega)) \tag{5}$$

Equation (5) and Fig. 7 imply that, $\mathbf{E}$ and $\mathbf{B}$ fields should have frequencies lower than the common radio and microwave bands, i.e. the first peak in $\chi_e''(\omega)$ graph, in order to decrease overall conductivity, hence attenuation. Furthermore, in non-radiating fields, there holds no relation such as $|\mathbf{E}|/|\mathbf{B}| = v$. Therefore, $\mathbf{B}$ can be substantially large. It also means that the energy does not have to be divided equally between the $\mathbf{E}$ and $\mathbf{B}$ fields, as it does in radiating fields.

A starting point to choose the appropriate operating frequency is to compare our problem with other MI applications. Knowing that the *index of refraction* (n) of EM waves in soil is ≈ 1.5 [38], the speed of EM waves in soil is given as $v = c/n \approx 2 \times 10^8$ m/s. Therefore, for distances of 10 m to 70 m and working frequencies of 2 kHz to 9 kHz, we have $k.r \in [0.006, 0.01]$ which falls in the non-radiating field domain and does not interfere with any licensed frequencies.

A. System Components and Circuits

Fig. 8 shows the basic elements of a MI communication system. Coil antennas are used at the transmitter (Tx) and receiver (Rx) sides. Coils have low radiation resistance and transmit very little real power. Therefore, they have low performance for radiation field. Instead, a coil antenna has a high reactive power going back and forth to the antenna and the surrounding space in each cycle. This is a desired property for MI, unlike typical RF systems in which reactive power is kept as low as possible.
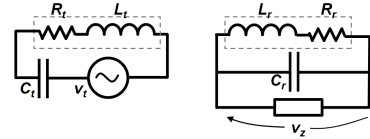

Fig. 8.   MI transmitter and receiver circuits

In comparing transmission power of MI and radio systems, one should note that unlike radio systems in which the consumed real power is transmitted and usually measured in dBm, a MI transmitter does not transmit real power. The consumed real power in a MI antenna is the wasted power in R_t as it is converted to heat. For instance, a commercial MI system might have a nominal power consumption between 100 W and 200 W which will be confusing if carelessly transformed into dBm scale.

Two coil transceivers operating at low frequencies can be viewed as a core-less transformer with two separate coils and inefficient coupling. Both coils can be fairly modeled as an ideal inductor in series with a resistor which is equal to resistance of the coil wire. We assume that the operating frequency is low enough, hence ignore the self capacitance across the coil in its lumped model. However, resistance of the coil wire depends on the operating frequency through *skin* and *proximity effects*.

At Tx side, the objective is to produce the strongest possible $\mathbf{B}$ field. This will be achieved when electrical current in the coil (I_t) is maximized. Therefore, a capacitor C_t should be connected to the coil in series and bring it to resonance such that $I_t = v_t/R_t$. In practice, when R_t is small, a voltage

source with low output impedance should be used to be able to provide the required current.

In order to increase I_t further, R_t should be reduced. It can be achieved by breaking the coil into several parallel coils, connecting some/all of the individual wire turns in parallel [39]. If the total DC resistance is R and the wire turns are to be grouped in N parallel coils, each with DC resistance of R/N, the overall resistance (R_t) will be equal to R/N^2.

Increasing I_t will increase the voltage across C_t which is equal to v_t transformed by the *quality factor* of the Tx coil. In practice, when I_t is in order of tens of milli-amperes, the voltage across C_t could rise up to tens of volts. Therefore, C_t should have a high breakage voltage. As we will see later in this paper, the maximum permissible voltage for C_t was the parameter which limited I_t in our experiments.

The Rx coil, on the other hand, should be sensitive to the slightest changes of the passing magnetic flux and produce the highest back-emf. The induced RMS emf v_r can be calculated in a multi-turn coil by:

$$v_r = \omega . \sum_{i=1}^{N_r} \left[\int_{A_i} \bar{\mathbf{B}} . \hat{\mathbf{n}} d(s) \right] \tag{6}$$

where ω is the angular frequency of I_t, A_i the area of individual turns of the Rx coil, N_r the number of turns of the Rx coil, and $\bar{\mathbf{B}}$ is the RMS magnetic field passing through the it. If $\bar{\mathbf{B}}$ has a constant amplitude at all the points on the Rx coil surface and is parallel to $\hat{\mathbf{n}}$, which has unit length and is perpendicular to the coil surface, (6) will be simplified as follows:

$$v_r = \omega . |\bar{\mathbf{B}}| . \sum_{i=1}^{N_r} A_i \tag{7}$$

which shows that $\sum_{i=1}^{N_r} A_i$ should be maximized in order to get the highest possible back-emf. Furthermore, if a capacitor C_r is connected to both ends of the coil such that it brings the coil into resonance (see Fig. 8), the followings hold:

$$C_r = \frac{1}{\omega^2 L_r}$$
$$v_z \approx \frac{1}{jC_r\omega} I_r = -j\omega L_r(\frac{v_r}{R_r}) \tag{8}$$
$$= -jQv_r$$

provided that the input impedance of the receiver amplifier/filter is very large and the *quality factor* (Q) of the coil is defined as $Q = \omega L_r/R_r$. Therefore, if the Rx coil has a high Q, the passive band-pass receiver circuit acts as a pre-amplifier.

Combining (7) and (8), the design objective in Rx antenna is to maximize the following expression:

$$\frac{L_r}{R_r} . \sum_{i=1}^{N_r} A_i \tag{9}$$

As another approach, coupling between transmitter and receiver antennas can be formulated as mutual inductance between the two coils [19]. In district heating and water distribution systems, it is possible to amplify mutual inductance

by employing pipes as ferromagnetic cores of the transceiver antennas. This will increase the self and mutual inductance in expense of adding core losses. We have shown in [8] that mutual inductance can be enhanced by several orders of magnitude when coils are wound around steel pipes. However, iron losses counteract mutual inductance enhancement, thus we have used non-metallic core coils throughout this article.

Employing intermediate coils as magneto-inductive waveguides is another technique to increase the mutual inductance in specific directions and is investigated in [40] and [41]. However, it is not practical in our problem to insert intermediate coils because of the lack of pipes accessibility at regular distance intervals.

B. Coil Antenna Design

Given a specific wire gauge R, and length l, an interesting problem is how to wind the coils such that the design criteria in Tx and Rx antennas are met. Assumptions on wire gauge and length are reasonable since they define cost and weight of the coils. They hold throughout this section.

We start by introducing the analytical expression for the $\mathbf{B}$ field in all points of space, created by a single turn current loop as shown in Fig. 9. The formula is derived by calculating magnetic vector potential first, and taking its curl to find $\mathbf{B}$ [42].

$$\mathbf{B}(r,z) = \frac{\mu I k}{4\pi\sqrt{ar^3}} \left[-(z-h)\left(K(k) - \frac{2-k^2}{2(1-k^2)} E(k)\right)\hat{\mathbf{r}} \right.$$
$$\left. + r\left(K(k) + \frac{k^2(r+a)-2r}{2r(1-k^2)}E(k)\right)\hat{\mathbf{z}} \right] \tag{10}$$
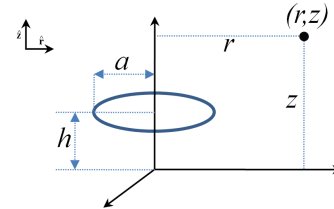

Fig. 9. A current loop

$\mathbf{B}$ is expressed in terms of complete elliptic integral functions of first and second kind, i.e. $K(k)$ and $E(k)$, where their argument k is defined as:

$$k = \sqrt{\frac{4ar}{(r+a)^2 + (z-h)^2}}$$

All other parameters of (10) are expressed in Fig. 9. If $\mathbf{B}$ is only sought on z-axis, (10) will be significantly simplified. In that case, it is more convenient to directly use Biot-Savart law to calculate on-axis $\mathbf{B}$ field.

1) Relative positioning of Tx and Rx antennas: The graphical representation of $|\mathbf{B}|$ for a multi-turn coil is given in Fig. 10 as a contour plot at two zoom levels. The coil is not shown in this plot, but it is laid in $z = 0$ plane and centered at the origin, with $a = 0.1$ m.

The field is calculated at each point in space by summing up (10) for individual wire turns, considering the exact radius and location for each turn of wire.

It is shown that $|\mathbf{B}|$ is larger around the coil and on the coil's axis. An interesting behavior is observed on $z = 0$ plane where $|\mathbf{B}|$ has a local minimum at a radius of approximately 2.4 a. This is due to the $\mathbf{B}$ field generated by the currents flowing in farther parts of the loop which counteract the $\mathbf{B}$ field generated by the currents flowing in the closer parts. At larger distances from the coil, $|\mathbf{B}|$ starts to degrade monotonically.
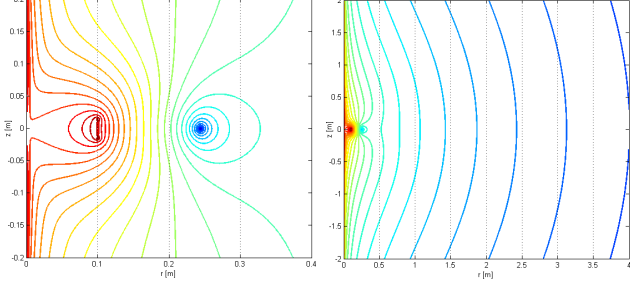

Fig. 10. Contour plots of $|\mathbf{B}|$ in the space surrounding the Tx antenna at two zoom levels

Since the contours in Fig. 10 (right) do not follow an exact spherical pattern, there are variations in $|\mathbf{B}|$ at fixed distances from the Tx antenna. It is clear that $|\mathbf{B}|$ is larger around the z-axis. This behavior is shown quantitatively in Fig. 10, in which $|\mathbf{B}|$ is drawn at three different fixed distances of 1 m, 10 m, and 100 m from the Tx antenna. Each curve starts from the vicinity of the z-axis, associated with $\theta = 0.1°$ to $z = 0$ plane, associated to $\theta = 90°$. The results are shown in log-log scale in sake of highlighting the differences. Moreover, the curves are shifted vertically such that they all coincide at $\theta = 90°$. Fig. 11 shows that $|\mathbf{B}|$ can vary up to approximately 20 dB at the Rx antenna based on positioning of the Tx antenna if $\theta \in [1°, 90°]$. It also shows that $|\mathbf{B}|$ is more sensitive when θ is small.
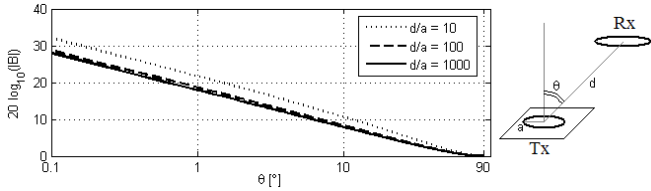

Fig. 11. Normalized $|\mathbf{B}|$ vs. Rx coil position with respect to Tx coil axis

Note that Fig. 11 does not give any information about the angles between Tx and Rx coils' axes, which is important in calculating the magnetic flux passing through the Rx coil.

2) Cross section shapes: Given the mean radius of the coil a, and hence the number of its turns N, $(N = l/(2\pi a))$, we have compared rectangular cross section shapes with different side proportions to see its effect on the Tx and Rx antennas. These are ranging from a single layered coil in which $b = 2R$ and $c = Rl/(\pi a)$ to a coil with the maximum number of winding layers which is made when $b \leq 2a$ and $c \geq R^2 l/(\pi a^2)$. The latter holds, provided that each wire occupies a square surface of area $4R^2$ at the cross section of the coil. The most compact wiring, results in hexagonal surface assignment to each wire turn and $c \geq \frac{\sqrt{3}R^2 l}{2\pi a^2}$. All of the above inequalities convert to equalities if the wire is very long such that no hole remains in the center of the multi-turn coil.
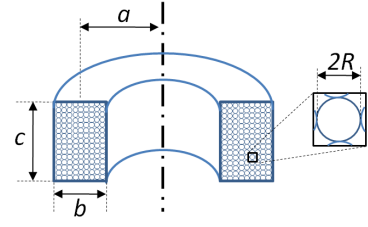

Fig. 12. Dimensions of a multilayer coil with rectangular cross section

At Tx coil, the difference between $|\mathbf{B}|$ of a single layer and a square coil at $z = 0$ plane is in order of 0.01% of the $|\mathbf{B}|$ created by either of them. In all other points in the space, this trifling difference is even more negligible. Therefore, the cross section shape of the Tx antenna is not tangibly influential on $|\mathbf{B}|$.

At Rx coil, on the other hand, the coil's cross section shape is quite influential mostly due to its effect on self inductance of the coil (L_r). This is explicitly presented in (9). Since the length and the mean radius of the coil are predefined, $\sum_{i=1}^{N_r} A_i$ is constant and L_r must be maximized.

Maximization of self inductance of a coil was first posed by Maxwell in [43]. He has shown that the *geometric mean distance* between the conductors of an inductor should be minimized in order to get the maximum inductance. This is achieved when the cross section is circular. For rectangular shapes which are easier to manufacture, the best shape is a square, i.e. $b = c$ (See Fig. 12). This result is verified by simulations in Fig. 13.
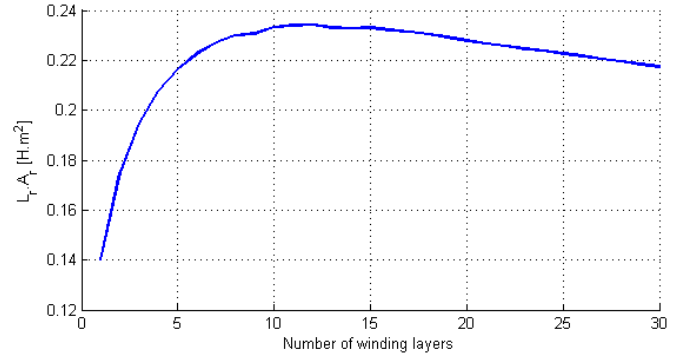

Fig. 13. emf variations in the Rx coil as a function of cross section shape

The coil in this simulation is made up with 150 m of wire with gauge $R = 0.3$ mm. Its cross section is rectangular and the mean radius is $a = 0.20$ m. Consequently, the number of turns N_r turns out to be 119 which yields 11 winding layers for a square cross section. Fig. 13 confirms this fact by showing a peak at $N_r = 11$. It also shows that a single layer Rx coil has only 60% performance of the square shaped Rx coil.

In the above simulation, L_r is calculated by injecting a current I into the receiver coil and computing the induced magnetic flux Φ_i in each turn due to the current in all of the turns. Then, $L_i.I = \Phi_i$ gives L_i and $L_r = \sum_{i=1}^{N_r} L_i$. Note that, in calculating the total self inductance of the Rx coil, we only added up L_i of individual turns which convey the self inductance of that turn plus its mutual inductance to all other turns.

3) Mean radius vs. Number of turns: Since the total wire length ($l = 2\pi a N$) is predefined, aN is constant and we

should make a trade-off between a and N. Fig. 14 illustrates the variations in $|\mathbf{B}|$ at $z = 0$ as r increases from 1 m up to 50 m, for different values of a from 0.03 m to 0.25 m at Tx antenna. The lowest value is associated with the physical limitation of $a > b/2$ (see Fig. 12 for clarification).
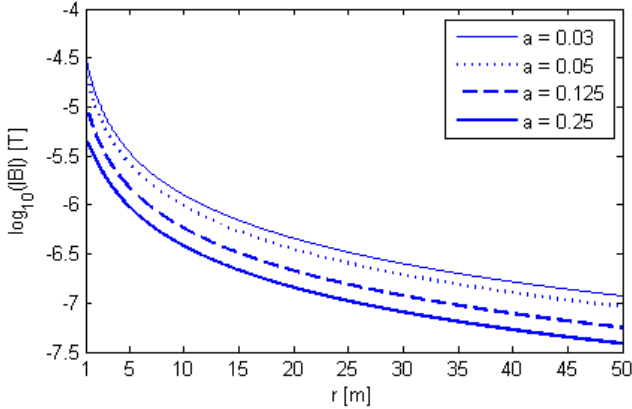

Fig. 14.   Variations in $|\mathbf{B}|$ as r increases

Fig. 14 suggests that a should be as small as possible to have the maximum $|\mathbf{B}|$ at large distances. The same results were achieved when $z \neq 0$ and also on any straight line with slope α such that $z = \alpha.r$. No matter how large a finite α is, the above hypothesis holds true and the smallest mean radius gives the maximum $|\mathbf{B}|$ at distances of interest. The only exception is $\alpha = \infty$, i.e. $|\mathbf{B}|$ on the z axis in which the converse is true, but it does not have any practical significance.

For Rx coil, expression (9) is depicted in Fig. 15 as a function of a. For all values of a, a square cross section is considered.
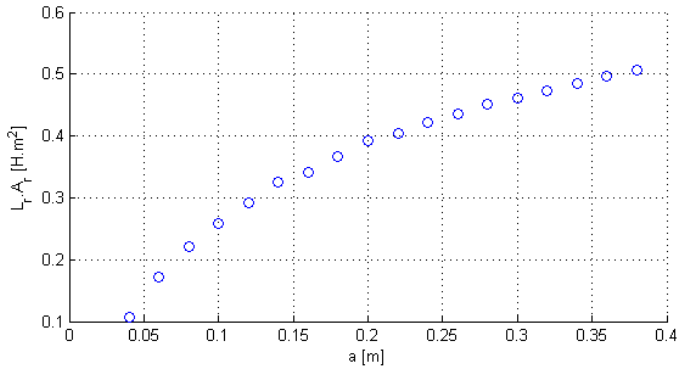

Fig. 15.   Variation in v_z at the receiver coil as a increases

Fig. 15 admits that for the Rx coil, larger a produces higher voltages, no matter if the number of turns or L_r is decreased significantly. In practice, a is usually specified by the space limitations. Moreover, Q of the Rx coil should be kept greater than 1, not to attenuate the signal. The presence of C_r capacitor is always necessary to adjust the phase of the received signal, such that it can be fed into an amplifier with resistive input impedance.

4) Summary of Coil Design Criteria:

- The Tx coil should have the smallest possible a while the Rx coil should have the largest possible a.
- The cross section of the Rx coil should be circular or square (when a circular shape is difficult to manufacture),

while the cross section shape of the Tx coil might be freely chosen based on practical winding issues.

Combining the above two statements suggests that the Tx coil should be single layered with a very large length (c) and $a = b/2$ which is impractical. Therefore, in practice, the maximum permissible length of the Tx antenna (c_{Max}) limits the size of the coil. As for the Rx coil, the maximum permissible radius (a_{Max}) specifies its size.

- The Rx coil center ought to be located on the Tx coil axis. Otherwise the attenuation in $|\mathbf{B}|$ could be approximated by the plot in Fig. 11.
- When the coils and their locations are known, the receiver should face the right direction such that $\mathbf{B}$ is perpendicular to the Rx coil surface. In worst case, when $\mathbf{B}$ and the coil's surface are parallel, nothing will be received at all.

IV. EXPERIMENTAL RESULTS

Having found the best conditions for Tx and Rx antennas, we investigated feasibility of communications in our district heating system. Feasibility study is done by planning a specific simulation scenario and comparing its results with actual measurements from an experiment with the same specifications.

A. Specifications and Assumptions

Three coils are used in our simulations and experiments with the following specifications listed in Tab. 1. Function of each coil is assigned with respect to the findings in the previous section.

TABLE I
COILS SPECIFICATIONS

Coil#	Coil 1	Coil 2	Coil 3
Wire length	148 m	359 m	142 m
Wire gauge	0.3 mm	0.35 mm	0.3 mm
Wire diameter incl. insulator	0.65 mm	0.80 mm	0.65 mm
Wire specific DC resistance	0.06 Ω/m	0.045 Ω/m	0.06 Ω/m
Wire measured DC resistance	8.90 Ω	16.19 Ω	8.90 Ω
Coil mean radius (a)	2.8 cm	30 cm	11.3 cm
Coil cross section shape	rect.	circ.	circ.
Coil width (b)	$\approx$3.3 mm	$\approx$12.5 mm	$\approx$10.5 mm
Coil length (c)	111 mm	$\approx$12.5 mm	$\approx$10.5 mm
No. of wire turns	841	190	200
No. of winding layers	5	N/A	N/A
No. of wire turns per layer	169	N/A	N/A
Function	Tx	Rx	Tx/Rx

Remark 1: It is assumed that $\mathbf{B}$, unlike $\mathbf{E}$ has a similar attenuation in air and in wet soil due to similar magnetic permeability in these environments. This is explained by the practical separation of $\mathbf{B}$ and $\mathbf{E}$ fields at non-radiating fields domain. Therefore, we have carried out all of the experiments in office environment, not in wet soil.

Remark 2: Operating frequency is chosen to be 5055$\pm$1 Hz for all three coils. Variable capacitors are connected to each of the coils and adjusted accurately to attain 5055 Hz resonance frequency. However, since the experiments are carried out in office environment, it is observed that the self inductance of the coils, and hence their resonance frequency is dependent

on surrounding ferromagnetic objects, e.g. office heating radiators. Therefore, re-adjustment of the capacitors is needed during experiments.

Remark 3: During experiments, an audio amplifier is used in connection with a digital signal generator at the Tx side to be able to provide the required electrical current. At the Rx side, an oscilloscope receives signals without any additional filter or amplifier.

B. Experiment 1 – Measured vs. calculated self inductance

The purpose of the first test was to verify if (10) in combination with the procedure introduced at the end of section III.*B.2* can be used to accurately calculate self inductance of a coil. Since only inductance of Rx coils are of interest in our simulations in the previous section, coil 2 and coil 3 are considered here. Calculated values are shown in Tab. 2 against actual values which are measured by two different methods. The first method involved direct use of a RLC-meter to measure L_r. The second method employed $L = 1/(4\pi^2 f^2 C)$ to find L based on using a known capacitor (C) in a LC circuit with our coil and measuring its resonance frequency by oscilloscope. The capacitor was connected in series with the inductor in this test for more accurate measurements in practice.

TABLE II
MEASURED VERSUS CALCULATED SELF INDUCTANCE

Coil#	Calc. L	Direct Meas. L	Indirect Meas. L
2	55.11 mH	54.5 mH	54.44 mH
3	18.37 mH	18.17 mH	18.12 mH

The results show only 1% difference between calculated and measured values which is satisfying.

C. Experiment 2 – Effect of Surrounding Ferromagnetic Objects

In this test, it was initially intended to verify that the received voltage across the Rx antenna (v_z) is a linear function of the electrical current in the Tx antenna (I_t) in practice, as it is evident from the Biot-Savart law. However, our observations suggest a different title for this experiment.
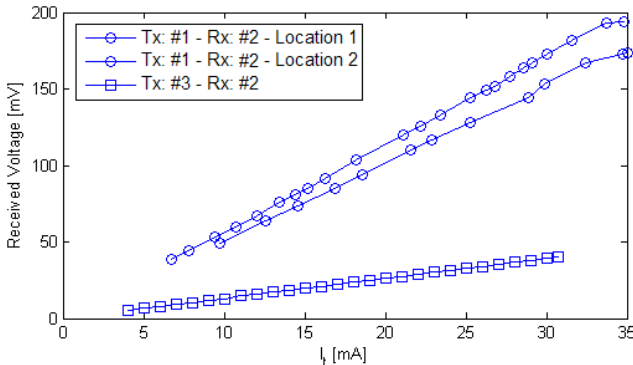

Fig. 16.   Received voltage as a function of Tx current

The test was planned for two combinations where either coil 1 or 3 are used as the Tx and coil 2 as the Rx antennas. Fig. 16 shows linear dependency between v_z and I_t for both cases. But the results were not easily reproducible. They varied if

nearby ferromagnetic objects were replaced, e.g. office chairs with iron parts. To visualize this effect, two graphs for coil 1 as the Tx antenna are plotted. Placement of the surrounding objects is quite different in one case from the other. All other parameters are unchanged. It can be seen that the slope of the line is changed. This experiment raises some concerns about the effect of steel pipes, in district heating systems, on the $|\mathbf{B}|$ field and self inductance of coils. More experimental studies or real scale implementations are needed to see whether this effect acts in favor or against our system in overall. The bottom line is that various physical piping layouts will impose an uncertainty in quality of the received signal.

D. Experiment 3 – Measured vs. calculated back-emf

This is the main experiment, in which we compared simulated and measured values of v_z. Based on (8) and backed by the promising results of Experiment 1, this test actually compares simulated and measured values of $|\mathbf{B}|$ at Rx side.

For coil 3 as the Rx antenna, (9) turned out to be 1.78572×10^{-2} H.m²/Ω. This value multiplied by ω^2, where the operating frequency is 5055 Hz, gives 1.80142×10^7 V/T which is voltage gain of the Rx coil. It is equal to the RMS of v_z if assuming: 1) a uniform $|\mathbf{B}|$ on surface of the Rx antenna, and 2) the ideal direction of the Rx antenna such that its surface is perpendicular to the $\mathbf{B}$ field.

Simulations and experiments are performed on $z = r$ cone. I_t is chosen such that peak-to-peak voltage across C_t does not exceed 40 V, i.e. the maximum permissible voltage for our capacitors. I_t turned out to be 31.0 mA and 28.8 mA RMS for coil 1 and coil 3, respectively.
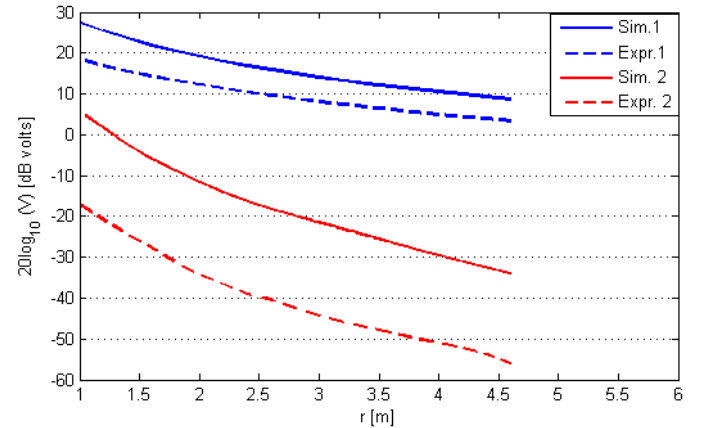

Fig. 17.   Calculated versus measured received voltage v_z for two Tx coils

Calculated and actual voltages are shown in Fig. 17. It is obvious that coil 1, as the Tx antenna, is superior to Coil 3 both in simulations and in practice. If we consider a detection threshold of 1 mV, i.e. -60dBm, the configuration with coils 3 and 2 is useful for no longer than 5 m links. However, the other configuration with coils 1 and 2 looks quite promising at this range. Even better results can be achieved by following coil antenna design criteria of the previous section, more precisely.

Unfortunately, the phenomenon that we observed in Experiment 2, affected this experiment as well. When distance increased, the results became less reproducible. That is why we have not plotted the graph for longer ranges. In summary,

the results are sensitive to presence of ferromagnetic objects between transceivers. Effects are not always destructive, and more advanced experiments are needed in order to commercialize this solution.

V. Conclusion

Among the investigated technologies for realizing communication links between pumps of a district heating system, power line communications and magnetic induction are the most viable options. The former has already found many competitive applications. The variety of applications has put off standardization activities. The latter has only been used in very specific domains so far, with high power consumption and extended ranges. It is anticipated in this article that this technology can be used with mild power requirements in underground urban utilities with relatively short range multi-hop networks. The bottom line is to systematically quantify effects of ferromagnetic materials in the vicinity of transceivers. Furthermore, since the operating frequency is very low compared to other RF solutions, available bandwidth is limited. This makes the solution not interesting for broadband applications. Therefore, MI is exclusively useful for sensor networks which require a small amount of bandwidth with guarantees of the availability of the channel as soon as it is needed.

References

[1] WIDE: Decentralized and Wireless Control of Large-Scale Systems, WP2 & WP5. [Online]. Available: http://ist-wide.dii.unisi.it

[2] Neptune project, WP1.1. [Online]. Available: www.shef.ac.uk/neptune

[3] WINES: Wireless Intelligent Networked Systems. [Online]. Available: http://www-civ.eng.cam.ac.uk/geotech_new/WinesInfrastructure/

[4] P³C: Plug and Play Process Control, WP1. [Online]. Available: http://vbn.aau.dk/en/projects/plug-and-play-process-control-p3c(cdd30235-5d31-4f94-bd17-c29028934471).html

[5] B. Bohm, N. K. Vejen, J. Rasmussen, N. Bidstrup, K. P. Christensen, F. Bruus, and H. Kristjansson, *EFP-2001 Fjernvarmeforsyning af Lavenergiomraader*, Energistyrelsen Technical Report, March, 2004, in Danish.

[6] Danfoss A/S, *The Heating Book - 8 Steps to Control of Heating Systems*, [Online]. Available: http://heating.danfoss.com/Content/61078BB5-1E17-4CA2-AC49-8A7CAC2BA687_MNU17424997_SIT54.html

[7] C. D. Persis and C. Kallesoe, "Pressure regulation in nonlinear hydraulic networks by positive controls," in *Proceedings of European Control Conference*, Budapest, Hungary, August, 2009, pp. 4102-4107.

[8] S. A. Meybodi, P. Pardo, and M. Dohler, "Magneto-inductive communication among pumps in a district heating system," in *the 9th International Symposium on Antennas, Propagation and EM Theory (ISAPE)*, Guangzhou, China, December, 2010, pp. 375-378.

[9] R. Bansal, "Near-field magnetic communication," *IEEE Antennas and Propagation Magazine*, **46**, 2, April, 2004, pp. 114-115.

[10] C. Bunszel, "Magnetic induction: a low-power wireless alternative," *Defense Electronics, Formerly: RFDesign*, **24**, 11, November, 2001, pp. 78-80.

[11] V. Palermo, P. J. Cobler, and N. R. Butler, "Inductive communication system and method," *United State Patent 7 254 366 B2*, August, 2007.

[12] J. Sojdehei, P. Wrathall, and D. Dinn, "Magneto-inductive (MI) communications," in *Oceans, MTS/IEEE Conference and Exhibition*, Honolulu, HI, USA, November, 2001, pp. 513-519.

[13] J. Sojdehei, F. Garcia, and R. Woodall, "Magneto-inductive seismic fence," *U.S. Patent 5 969 608*, October, 1999.

[14] R. Batcher, "Loop antenna for submarines," *Wireless Age*, **7**, p. 28, 1920.

[15] D. Reagor and J. Vasquez-Dominguez, "Through-the-earth radio," *U.S. Patent 7 149 472*, December, 2006.

[16] I. Akyildiz and E. Stuntebeck, "Wireless underground sensor networks: Research challenges," *AdHoc Networks Journal*, **4**, 6, November, 2006, pp. 669-686.

[17] M. Hallikainen, F. Ulaby, M. Dobson, M. El-Rayes, and L. Wu, "Microwave dielectric behavior of wet soil – part I: Empirical models and experimental observations," *IEEE Transactions on Geoscience and Remote Sensing*, **GE-23**, 1, January, 1985, pp. 25-34.

[18] M. C. Dobson, F. T. Ulaby, M. T. Hallikainen, and M. A. El-Rayes, "Microwave dielectric behavior of wet soil – part II: Dielectric mixing models," *IEEE Transactions on Geoscience and Remote Sensing*, **GE-23**, 1, January 1985, pp. 35-46.

[19] I. Akyildiz, Z. Sun, and M. Vuran, "Signal propagation techniques for wireless underground communication networks," *Physical Communication*, **2**, 3, September, 2009, pp. 167-183.

[20] P. Kyosti, J. Meinila, L. Hentila, X. Zhao, T. Jamsa, C. Schneider, M. Narandzic, M. Milojevic, A. Hong, J. Ylitalo, V. Holappa, M. Alatossava, R. Bultitude, Y. de Jong, and T. Rautiainen. (2008, 2) *WINNER II Channel Models, Part I, D1.1.2 V1.2*. [Online]. Available: http://www.ist-winner.org/WINNER2-Deliverables/D1.1.2.zip

[21] O. Tonguz, A. Xhafa, D. Stancil, A. Cepni, P. Nikitin, and D. Brodtkorb, "A simple path-loss prediction model for HVAC systems," *IEEE Transactions on Vehicular Technology*, **53**, 4, July, 2004, pp. 1203-1214.

[22] M. H. Nayfeh and M. K. Brussel, *Electricity and Magnetism*, New York, John Wiley & Sons Inc., 1985.

[23] (2010, August) Wikipedia: Electrical conductivity. [Online]. Available: http://en.wikipedia.org/wiki/Electrical_conductivity

[24] R. Long, P. Cawley, and M. Lowe, "Acoustic wave propagation in buried iron water pipes," in *Proceedings of the Royal Society, A: Mathematical, Physical & Engineering Sciences*, **459**, 2039, November, 2003, pp. 2749-2770.

[25] M. Stojanovic, "Underwater acoustic communications: Design considerations on the physical layer," in *the IEEE Fifth Annual Conference on Wireless on Demand Network Systems and Services (WONS)*, Garmisch-Partenkirchen, January, 2008, pp. 1-10.

[26] I. F. Akyildiz, D. Pompili, and T. Melodia, "Underwater acoustic sensor networks: research challenges," *Elsevier Ad Hoc Networks*, **3**, 3, May, 2005, pp. 257-279.

[27] H. Sakuma, K. Nakamura, and S. Ueha, "Two-way communication over gas pipe-line using multicarrier modulated sound waves with cyclic frequency shifting," *Acoustical Science and Technology, The Acoustical Society of Japan*, **27**, 4, July, 2006, pp. 225-232.

[28] H. Sakuma and J. Fujiwara, "Acoustic communication device and acoustic signal communication method," *U.S. Patent 7 027 357 B2*, April, 2006.

[29] A. Kondis, *Acoustical Wave Propagation in Buried Water Filled Pipes*, Master's thesis, Massachusetts Institute of Technology, February, 2005.

[30] G. Kokossalakis, *Acoustic Data Communication System for In-Pipe Wireless Sensor Networks*, Ph.D. dissertation, Massachusetts Institute of Technology, February, 2006.

[31] Y. Sherif and S. Zahir, "On power-line carrier communication (PLC)," *Microelectronics and Reliability*, **24**, 4, April, 1984, pp. 781-791.

[32] R. Arrington, "Load management and automatic meter reading through the use of power line carrier," *Electric Power Systems Research*, **4**, 2, April, 1981, pp. 85-104.

[33] D. Clark, "Powerline communications: finally ready for prime time?" *IEEE Internet Computing*, **2**, 1, January, 1998, pp. 10-11.

[34] S. Galli, A. Scaglione, and Z. Wang, "For the grid and through the grid: The role of power line communications in the smart grid," *Proceedings of the IEEE*, **99**, 6, June, 2011, pp. 998-1027.

[35] R. G. Olsen, "Technical considerations for wideband powerline communication – a summary," in *IEEE Power Engineering Society Summer Meeting*, **3**, Chicago, IL, USA, July, 2002, pp. 1186-1191.

[36] K. Erickson, A. Miller, E. Stanek, C. Wu, and S. Dunn-Norman, *Pipelines as Communication Network Links*, Technical Report at University of Missouri-Rolla, March, 2005.

[37] C. A. Balanis, *Advanced Engineering Electromagnetics*, New York, John Wiley & Sons Inc., 1989.

[38] T. Ishida, H. Ando, and M. Fukuhara, "Estimation of complex refractive index of soil particles and its dependence on soil chemical properties," *Elsevier Remote Sensing of Environment*, **38**, 3, December, 1991, pp. 173-182.

[39] E. Locke, "Switchable transceiver antenna," *U.S. Patent 6 333 723*, December, 2001.

[40] Z. Sun and I. Akyildiz, "Underground wireless communication using magnetic induction," in *In Proceedings of IEEE International Conference on Communications (ICC)*, Dresden, Germany, June, 2009, pp. 1-5.

[41] Z. Sun and I. Akyildiz, "Magnetic induction communications for wireless underground sensor networks," *IEEE Transactions on Antennas and Propagation*, **58**, 7, July, 2010, pp. 2426-2435.

[42] K. Kuns, *Calculation of Magnetic Field Inside Plasma Chamber*, Technical Report at University of California Los Angeles, August, 2007.

[43] J. C. Maxwell, *A Treatise on Electricity and Magnetism, Volume 2*, Oxford, Clarendon press, 1873.